

First simultaneous detection of helium and tritium inside bubbles in beryllium

M. Klimenkov^{a,*}, P. Vladimirov^a, J. Hoffmann^a, N. Zimmer^a, A. Möslang^a, V. Kuksenko^b

^aKarlsruhe Institute of Technology (KIT), Institute for Applied Materials-Applied Materials Physics (IAM-AWP), Hermann-von-Helmholtz-Platz 1, 76344 Eggenstein-Leopoldshafen, Germany

^bCulham Centre for Fusion Energy, Culham Science Centre, Abingdon, Oxfordshire OX14 3DB, United Kingdom

ARTICLE INFO

Keywords:

EELS
Bubble
Beryllium
Tritium
Hydrogen
Helium

ABSTRACT

Electron energy loss spectroscopy (EELS) was applied to detect and analyze quantitatively helium (He) and tritium (³H) enclosed inside bubbles in irradiated beryllium. Both gases were formed in beryllium under neutron irradiation as a consequence of neutron-induced transmutation reactions. They were detected for the first time as pronounced peaks at 13.0 eV for ³H and 22.4 eV for He in EELS spectra collected from flat hexagonal bubbles. An adhesion of ³H or formation of thin beryllium hydride layers on the internal basal surfaces was observed. The number densities of both gases were estimated using electron scattering cross-section and intensities obtained from EELS spectra. The number density values estimated for various bubbles fluctuate from 4 to 15 at/nm³ for He and from 4 to 10 molecules/nm³ for ³H₂. Lower gas number density was measured inside large bubbles. The observed higher density of tritium at inner walls of bubbles seems to confirm very recent *ab initio* calculations of the interaction of hydrogen isotopes with beryllium surfaces.

1. Introduction

The local detection and analysis of elements with lowest atomic numbers, (Z) such as hydrogen (H) and helium (He) using electron energy loss spectroscopy (EELS) in transmission electron microscopy (TEM) is a challenging task. These two elements obey comparatively small scattering cross sections and their energy loss edges at 13.2 eV for H₂ molecules (K edge) and 22.4 eV for He atoms (He K edge) are in the range of typical plasmon energies for beryllium (Be) or other elements as well. Being the smallest atom, hydrogen readily dissolves in metals interstitially but its fast diffusion hinders formation of bubbles with considerable gas density. The standard H₂ and He K lines provided in the EELS atlas were obtained by filling the TEM chamber with these gases at low pressure (Ahn et al., 1983; Crozier and Chenna, 2011). Only few articles report possible presence of hydrogen in closed gas bubbles (Blackmur et al., 2018; Leapman and Sun, 1995; Lu et al., 2018), however, the H line is quite weak and visible as a shoulder on the plasmon peak. Blackmur et al. (2018) demonstrate the presence of a line at 13.4 eV around spherical bubbles formed in He and H implanted zirconium. However, the authors were not certain concerning the origin of the “13 eV” line. Both, cavity plasmon oscillation as well as H adsorption on thermal walls were considered for its explanation.

Hydrogen bound in hydrides or hydroxides does not give rise to any

core loss edges that can be used for detection by EELS (Paik et al., 2010; Tao et al., 2013). Dissolved in a metallic matrix, hydrogen atoms give up their electrons that join the valence band and become loosely bound protons. The indirect way to demonstrate the presence of hydrogen inside solid state is to show changes in the plasmon structure (Hojou et al., 1998). The weak pre shoulder on low energy side of plasmon could be considered as indication for H adsorption on internal bubble walls in SiC material (Hojou et al., 1998).

The second indirect way is to use the high sensitivity of hydroxides or organic compound to the electron beam. O–H bonding in the solids is weaker than O metal bonding forming gaseous oxygen, which can be identified based on the fine structure of O–K edge (Klimenkov et al., 2008). The direct EELS measurement of hydrogen is herewith only possible when it forms H₂ molecules inside bubbles. In the last decades, slightly more than a dozen articles on the detection of hydrogen in the solid state using EELS were published. Most of these publications describe the appearance of H₂ in organic materials, hydrides or hydroxides or in lithium compound (Cohen et al., 2015; Jiang et al., 2018; Lu et al., 2018; Yakovlev et al., 2009).

The detection of helium using EELS has been much frequently discussed in the scientific literature. Helium is practically insoluble in metals and tends to precipitate into nanoscale bubbles. Already in 1982, two methods for evaluation of the He density in bubbles

* Corresponding author.

E-mail address: michael.klimenkov@kit.edu (M. Klimenkov)

produced by ion implantation were proposed (Jäger et al., 1982; Manzke et al., 1982; Walsh et al., 2000). The calculated total scattering cross section and the blue shift of the He K line inside gas bubbles were used for the estimation of the gas density. However, the later method can only be applied to bubbles with sizes of less than 7 nm which contain sufficiently large He density (Fréchard et al., 2009). For larger bubbles, density measurements can be performed more reliably by the detection of the line intensity and subsequent calculation of the scattering cross section (Walsh et al., 2000). However, a direct detection and analysis of different coexisting light gases inside bubbles or voids in hexagonal closed packed metals like beryllium (Be) was not reported so far.

Helium and tritium (^3H) are produced in beryllium, as consequence of n induced transmutation reactions. Beryllium is considered as a potential neutron multiplier material for the helium cooled pebble bed blanket concept (HCPB) of the international thermonuclear experimental reactors (ITER) (Barabash et al., 2011; Vladimirov et al., 2014), where it will be exposed to a high neutron irradiation dose. Both gases have rather low solubility in metals and, being mobile at elevated temperatures, precipitate in the form of gas bubbles resulting in such detrimental effects as swelling, severe loss of ductility and material embrittlement (Klimenkov et al., 2013a,b; Möslang and Wiss, 2006). The most detrimental effect for beryllium is the ^3H retention, which can reach 7 kg for 300 tons of Be pebbles required for HCPB blanket. The proof for helium and hydrogen retention inside beryllium was provided by gas release experiments (Chakin et al., 2013; Chakin and Ye Ostrovsky, 2002). The pronounced increase in gas release near melting temperature (~ 1500 K) was interpreted as simultaneous release of He and ^3H . However, the detection and analysis of gases inside bubbles in beryllium was never performed quantitatively, e.g. by analytical transmission electron microscopy. The main focus of the previous TEM studies was on the characterization of the bubbles, determination of their shapes, dimensions and number density as well as evaluation of the microscopic swelling (Klimenkov et al., 2013a, 2014; Rabagliano et al., 2003). In Refs. (Klimenkov et al., 2013a, 2014), it was reported that gas bubbles have a hexagonal coin like shape whose diameter and thickness strongly depend on the irradiation temperature. Neutron irradiation at 648 K leads to the formation of bubbles with a diameter of typically 10 nm. Their size increases up to 80–150 nm at 948 K (Klimenkov et al., 2013a). In the present publication, we demonstrate the possibility of detecting and quantitatively analyzing He and $^3\text{H}_2$ inside gas bubbles using EELS in STEM. Finally, the observed, characteristic density distribution of $^3\text{H}_2$ provides also a first experimental indication for the existence absorption of hydrogen isotopes at the inner (0001) surfaces of Be recently predicted by a multiscale modelling approach based on *ab initio* Molecular Dynamics and Kinetic Monte Carlo simulations (Stihl and Vladimirov, 2016).

2. Experimental

In the present study, beryllium was used in the form of pebbles with diameters of ~ 1 mm produced by the rotation electrode method. Their microstructure before and after irradiation was described in detail in previous publications (Chakin et al., 2013; Klimenkov et al., 2013a; Vladimirov et al., 2015). The pebbles analyzed in this study were irradiated within the high dose Be irradiation program (HIDOBE II) in the High Flux Reactor in Petten, Netherlands at $T_{\text{irr}} = 968$ K up to a dose of 37 displacements per atom (dpa). The calculated helium production was estimated to be 6000 appm He. The calculation of transmutation reactions shows that in beryllium different isotopes such as ^3He , ^4He , and ^3H are formed (Sernyaev, 2001). As the same chemical elements isotopes cannot be distinguished by EELS, they will be denoted as He and H when considering EELS spectra.

The irradiated pebbles were embedded in a resin and mechanically polished. Afterwards, thin lamellae were prepared using focused ion beam (FIB) technique. Beryllium is rather transparent for electrons with

200 eV energy, as it is characterized by inelastic mean free path of 160 nm for 200 kV electrons (Iakoubovskii et al., 2008). Consequently, it appears possible to image details in Be foils with thicknesses of up to 400 nm. The lamellae were examined using a Tecnai™ G2 transmission electron microscope (FEI Company) equipped with an EDAX Si Li detector for energy dispersive X ray spectroscopy (EDX), a Gatan Tridiem 863 post column image filter (GIF) and a scanning unit (STEM) with high angle annular dark field (HAADF) detector. EELS and EDX analyses were performed using the STEM mode obtaining a spectrum in each point. The energy dispersion of 0.2 eV per channel was used for the EELS spectroscopy. The spatial resolution for these investigations was ~ 1 nm. The probe convergence semi angle with the 50 μm aperture was 9 mrad and collection semi angle was ~ 11 mrad. The maximum possible tilting of the goniometer was from $\sim +33^\circ$ to $\sim -33^\circ$. The microscope is located in the hot cells facility of the Fusion Materials Laboratory (FML) at KIT with the possibility of working with radioactive materials. The calculation of the partial inelastic cross section was performed using the Sigmap3 program provided in the ref. (Egerton, 2011).

3. Results

3.1. Characterization of irradiated Be

The microstructure of beryllium after neutron irradiation is characterized by formation of bubbles with diameters of up to 250 nm inside grains and up to several microns on the grain boundaries (Chakin and Ye Ostrovsky, 2002; Klimenkov et al., 2013a). In good agreement with previous investigations, the bubbles in irradiated Be are formed on the basal planes and have the shape of hexagonal coins, which dimensions such as diameter and thickness will be used further in the manuscript when describing the bubbles (Klimenkov et al., 2013a). This particular lamella prepared from the intergranular area obey a thickness, which increases from 120 nm on the edge to 350 nm on the thickest transparent area. The same area, which was taken from different viewing angles and differing by 65° (from -32° to $+33^\circ$ in the goniometer), is imaged in two micrographs (Fig. 1a,b). The bubbles are displayed as ovals (a) and as flat rectangles (b). In Fig. 1c e, the schematic drawing shows the lamellae for different goniometer orientations. In the TEM image with oval bubbles (Fig. 1a), the (0001)_h direction forms an angle of 60° to the image plane (schematic view in part (d)). If the (0001)_h axis is directed in the image plane (Fig. 1e), the bubbles are displayed as narrow rectangles (on edge orientation). The bubbles could also be imaged as hexagons if the (0001)_h direction is parallel to the electron beam (planar orientation of the disks). Between on edge and planar orientations, the bubbles are mainly visible as ovals (Fig. 1a).

Acquiring EELS spectra with sufficient signal to noise ratio for the He and H detection were only possible with an on edge orientation of the bubbles. However, with such orientation numerous bubbles are cut by the foil surface. The bubbles are naturally open with the consequence, that beryllium oxide (BeO) layers form immediately on the internal bubble surface when it contacts air. The open bubbles are then visible in HAADF images with bright frames due to the Z contrast (Fig. 2a) or in O K elemental EDX maps (Fig. 2b). The several “closed” bubbles, which are invisible in O K map are marked with arrows in the two images. From the 156 bubbles visible in Fig. 2a, only 36 are closed after preparation. Most of the closed bubbles have a size of less than 60 nm, however the best analytical results were achieved on the bubbles with diameters larger than 100 nm. The fraction of bubbles larger than 100 nm is about 25%. It is necessary to have lamellae thicker than 200 nm in order to have several closed bubbles with sizes larger than 100 nm. On the other hand, the foil thickness should not be larger than 1.5 of the mean free path of inelastic electron scattering (~ 250 nm) in order to obtain evaluable EELS spectra.

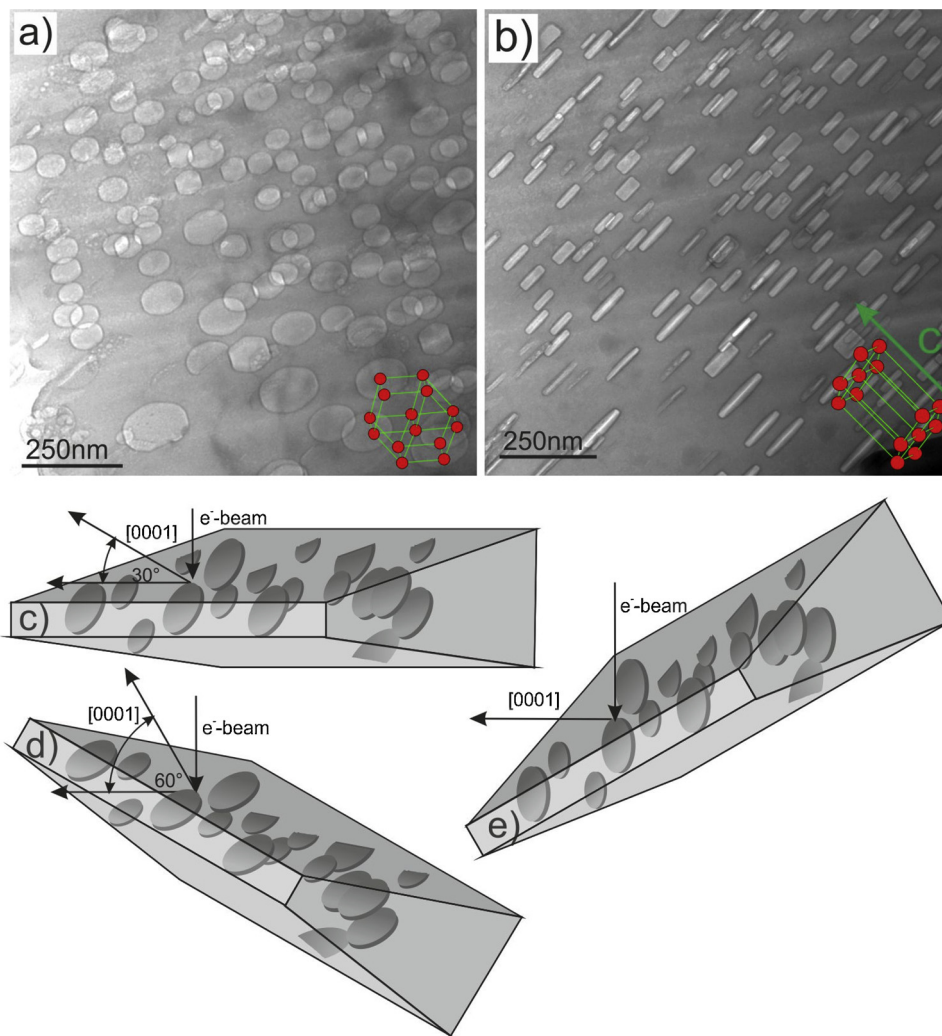


Fig. 1. Two images of the same area obtained with a 60° tilt difference provide an overview about microstructure of investigated material. The schematic drawing explains the orientation of (0001)_h axis and bubbles for different goniometer tiltings.

3.2. EELS investigation

The results of the analytical investigations of the 160 nm large bubble in on edge orientation are presented in Figs. 3 6. The thickness of the Be foil was measured to be 235 ± 25 nm (1.4λ) in the area next

to the bubble and 0.4λ (65 nm) inside the bubble. It is visible with a dark contrast, whereas all other bubbles around have a bright rim in the HAADF image, which indicates that the bubbles are open. Fig. 3b shows a series of low energy EELS spectra obtained across the bubble. The typical plasmon peak of metallic beryllium shows a maximum at

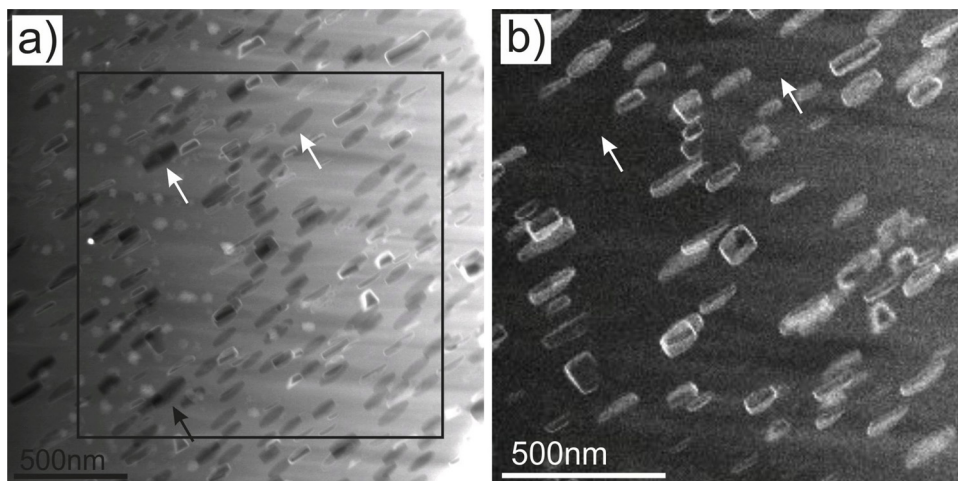


Fig. 2. HAADF image of the bubbles (a) and oxygen elemental map of the marked area (b). The positions of closed bubbles are marked by arrows in the both images.

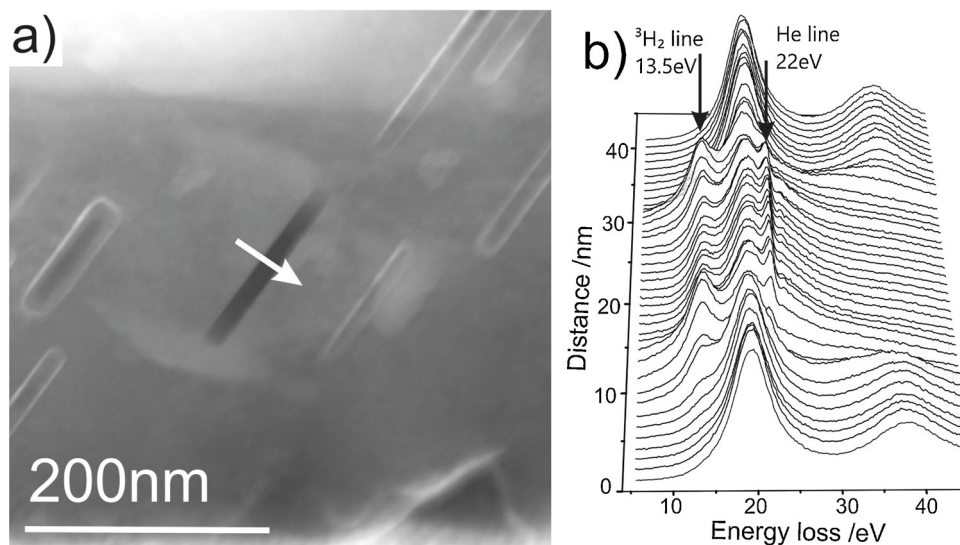


Fig. 3. HAADF image of the closed bubble (a) and individual spectra (b) from the STEM-EELS line scan along the beam path indicated in (a).

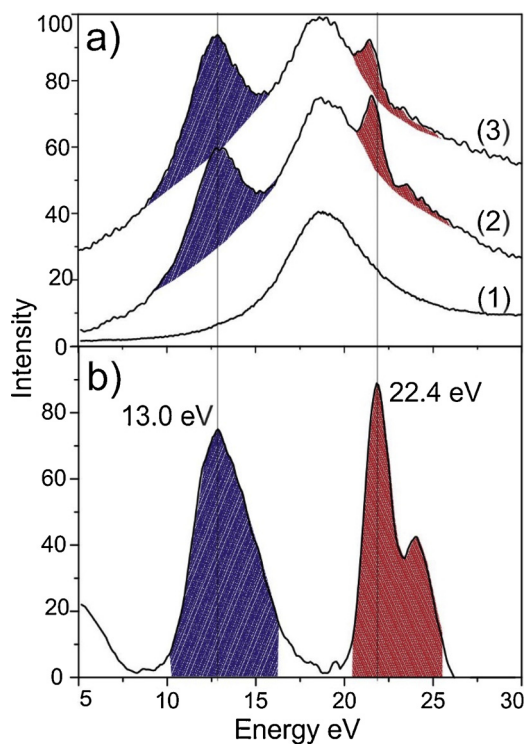


Fig. 4. Three individual spectra obtained from the line scan series in Fig. 3. (1) spectrum was taken from the matrix neat the bubble, whereas the (2) and (3) spectra were taken from the middle of the bubble and the interface respectively. The intensities of the H and He edges after background subtraction are shown in the part (b).

18.9 eV (Ahn et al., 1983). The spectra obtained next to the bubble show multiple plasmon peaks occurring with increase of thickness, where the second peak appears at 38 eV. The presence of pronounced H₂ at 13.0 eV and He at 22.4 eV lines on the left and right shoulders of plasmon peak can be seen in the spectra. The line energies for these two elements correspond to the energies given in Ref. (Ahn et al., 1983). Obviously, the intensity of the H₂ lines increases at the bubble's internal surface.

Three original spectra taken from different regions in the line scan experiment are drawn in Fig. 4a. Spectrum (1) was taken from the area in the immediate vicinity of the bubble, spectrum (2) directly from the

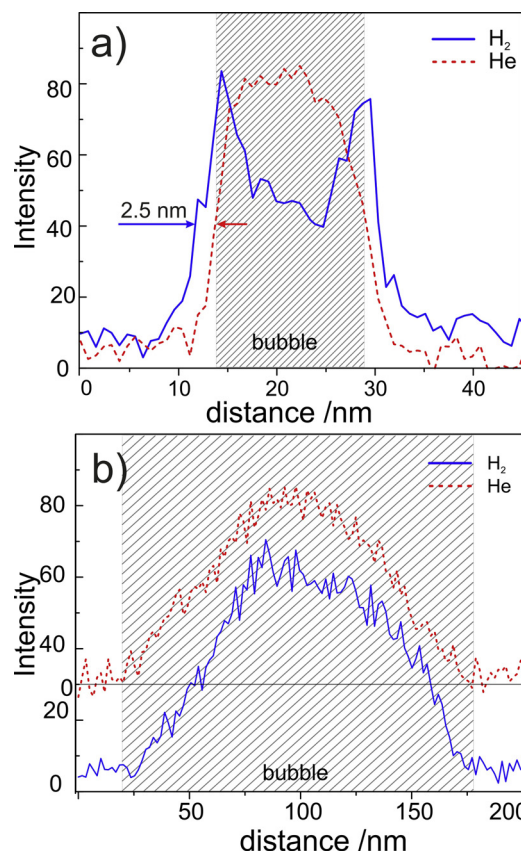


Fig. 5. The line profiles of H (blue solid curves) and He lines (red dashed curves) across (a) and along (b) the bubble.

bubble center and spectrum (3) from the internal bubble gas interface. The Be plasmon from the area next to the bubble was considered as background after multiple scattering correction. Fig. 4b shows the H and He lines after background subtraction. In the He line both 1s→2p and 1s→3p transitions are clearly visible.

Fig. 5 exhibit the intensity profiles of H₂ and He lines across (a) and along (b) the bubble. The profiles suggest that both gasses homogeneously fill the bubble. The intensity of the H₂ line increases on the internal basal surfaces (Fig. 5a).

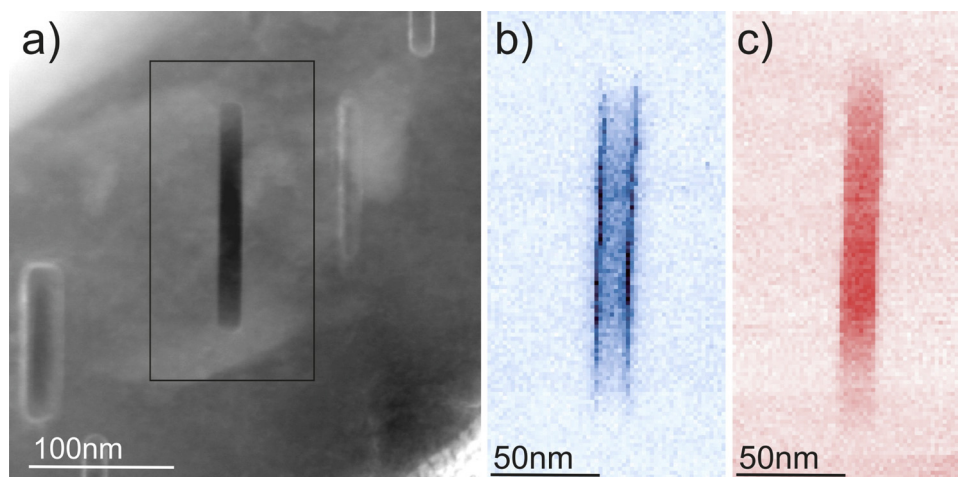


Fig. 6. A HAADF image of a bubble (a) and two dimensional intensity distributions of H (b) and He (c) lines.

A two dimensional distribution of H_2 and He line intensities is shown in Fig. 6. The spatial distribution of He shown in Fig. 6c is in agreement with the bubble thickness. The intensity increase of H line at the internal bubble surfaces is clearly visible in the H map. It can be estimated that approximately 30%–40% of the integrated H intensity is caused by hydrogen that occupies the internal basal planes of the bubbles.

4. Discussion

4.1. EELS detection of He and H_2 inside bubbles

Helium and heavy hydrogen isotope, tritium, are abundantly generated in beryllium under neutron irradiation. Although, the exact trapping sites of tritium were not undoubtedly determined experimentally so far, some facts are in favor of trapping at helium bubbles. In particular, temperature programmed desorption (TPD) experiments revealed simultaneous release of tritium and helium (Chernikov et al., 1996). This fact taken together with microstructural investigations (Chernikov et al., 1996; Pajuste et al., 2011; Vladimirov et al., 2015) allows to suggest that this simultaneous burst release occurs through the growth of bubbles until they overlap with each other and form in interconnected network of open channels reaching outer surface. In this moment simultaneous release peaks of He and T are registered in TPD experiments.

Beryllium, despite its low Z number, shows a high stability under electron beam and its low electron scatterings cross section insures optimal signal to noise ratio by analytical studying of closed bubbles. The on edge orientation, as is shown in Figs. 1c and 2 b, allows the examination of a 160 nm thick gas bubble surrounded by Be layers of only 10–20 nm on both sides. The probability to find a filled bubble enclosed in such a thin foil is relatively low. Consequently, the majority of the large bubbles with on edge orientation are open and visible in the HAADF images as well as in O K maps because the internal surface oxidizes easily when exposed to air (Fig. 2b).

The spectra plotted in Fig. 3b and 4 a show a sufficient intensity of He and H lines for their identification and analysis. The shape of both lines are in good accordance with EELS spectra recorded from gaseous H_2 and He (Ahn et al., 1983; Blackmur et al., 2018). The matching intensity profiles of both lines along and across the bubble reflect the bubble thickness, and hence the thickness of the measured gas volume (Fig. 4c). The increasing intensity of the H line on both basal planes indicates either preferential absorption of H at these surfaces or the formation of Be hydride at the internal walls (Figs. 3b, 4 b and 6). This effect was not observed on prismatic planes although they were not so nicely aligned with electron beam as the basal ones (Fig. 5b). To our

knowledge, the present study is the first one which shows a direct proof for the presence of He and H_2 inside bubbles formed in neutron irradiated beryllium. However, analytical TEM studies performed on materials containing either H_2 or He bubbles were published in the past (Frécharde et al., 2009; Leapman and Sun, 1995)

It was already shown, that implanted or transmutation induced He forms bubbles with detectable density in different classes of materials. The presence of the He lines in the region of the plasmon peaks, which corresponds to the $1s \rightarrow 2p$ (~ 22.4 eV) and $1s \rightarrow 3p$ (~ 24.6 eV) transitions in He atoms, was reported in several publications (David et al., 2014; Frécharde et al., 2009; Klimenkov et al., 2013b; Walsh et al., 2000). Quantification of helium inside bubbles was carried out in two ways: by measuring of the blue shift in the He $1s \rightarrow 2p$ line (Frécharde et al., 2009) and using scattering probability of electrons (Walsh et al., 2000). The first method was successfully applied to the over pressurized bubbles, which are filled with He achieving a density of up to 200 atoms/nm³. The size of such bubbles is typically less than 7 nm. The blue shift of the He line was observed then in the 1–3 eV range. The second, integration method described by (Egerton, 2011; Walsh et al., 2000) can be applied for the measurement of the gas density in any bubble, where a gas signal could be detected with sufficient signal to noise ratio.

The H assisted formation of voids and growth of H_2 filled bubbles in metals was widely studied in the past (Condon and Schober, 1993). The H_2 pressure inside was considered as an equilibrium state between bulk concentration and diffusion of H atoms from the one side and surface dissociation and gas pressure inside the bubble from the other side. It was assumed that a high H_2 amount inside bubbles can be achieved only due to chemisorption at the internal walls (Condon and Schober, 1993). The high solubility and diffusivity of H atoms inside solid states should prevent formation of bubbles filled with a large amount of H_2 gas, sufficient for direct detection. Actually, the direct detection of H_2 inside bubbles formed in solids using EELS has been reported in the literature only a few times. The pronounced H_2 EELS signal with a maximum at 13.0 eV with a threshold at 12.3 eV has been detected analyzing beam damage effects in organic material (Leapman and Sun, 1995). The quantification of H_2 line performed by integration method reveal the number density value of H_2 molecules $n(H_2) = 100 \text{ nm}^{-3}$. In a second study H_2 has been detected inside bubbles formed in hydrogenated Ti_2O shell (Lu et al., 2018).

4.2. Quantification of He and H

The quantification of both, He and H_2 inside bubbles was conducted by an integration method, which allows a direct determination of the number density of the gas atoms inside individual bubbles (Walsh et al.,

2000). For this purpose, the line intensities were taken from the spectrum in the middle of the bubble. The number density of element x (where x is He or H) is given by:

$$n_x = \frac{I_x}{I_z * d * \sigma_x}, \quad (1)$$

where I_z and I_x are integrated intensities of zero loss peak and He (or H) lines after background subtraction, $\sigma_p(\Delta, \beta)$ is the partial inelastic cross section for He $1s \rightarrow 2p$ (or H_2) line and d is the bubble thickness in the direction of electron beam. The cross sections for He K and H_2 lines $\sigma_p(\Delta, \beta)$ were calculated using the program Sigmak3 (Egerton, 2011). The collection semi angle β was 11 mrad and the integration range was 3 eV for both elements, which gives a values of cross sections of $6.7 \cdot 10^{-24} \text{ m}^2$ for He and of $5.8 \cdot 10^{-24} \text{ m}^2$ for H respectively. It was assumed that both gases behave as an ideal gas and pressure inside each individual bubble can then be determined by:

$$p = (n_{\text{He}} + n_{\text{H}_2})k_B T, \quad (2)$$

where n_x represents the calculated number densities for both gases, k_B the Boltzmann's constant and T the room temperature (293 K) (Leapman and Sun, 1995).

Fig. 4 shows the original spectrum from the middle of the bubble (a) and a spectrum after background subtraction (b). The plasmon peak from the area outside the bubble has been used for the background subtraction. The height of the peak was scaled to the height of the original spectrum. The results of quantification are shown in the Table 1. The uncertainty in the calculation of the number density was estimated to be about 30% for He and 35% for H. On one hand this error is caused by 15% uncertainty in the cross section calculations using the hydrogenic model (Egerton, 2011). On the other hand, we got 7% uncertainty in the values for He and 15% for H lines by the variation of the initial conditions for the background calculation and ~10% uncertainty in the sample thickness determination. The uncertainty for the total pressure inside bubbles is then estimated to ~30%. Despite the observed uncertainties, an obvious tendency towards an increase of the gas number density and pressure with decreasing bubble diameter can be derived.

The measured number densities of He and H_2 are low compared to other published results in other materials. It should be mentioned, that the bubbles have been formed and filled with both gasses during neutron irradiation. The total gas pressure under irradiation conditions should be 3 times higher than at room temperature. The results of He quantification inside bubbles shows, that they are often over pressurized. The He number density in such bubbles is much higher than the number density of liquid helium at 4.2 K (19 atoms/nm³). Under such conditions, the outer electron shell of He atoms is strongly deformed, resulting in an effect which could be detected as "blue shift" in EELS spectra (Fréchard et al., 2009). Typically a number density in the range of 30–140 atoms/nm³ inside He bubbles was reported (Fréchard et al., 2009; Walsh et al., 2000). In (Jäger et al., 1982) the values reach up to 200 atoms/nm³, which corresponds to a blue shift of ~5 eV. The H_2 number density inside bubbles was estimated only in one publication, where it was measured to $n(H_2) = 200 \text{ atoms/nm}^3$ (Leapman and Sun, 1995). It should be mentioned, that in all these cases, with exception of the last which reports the H_2 concentration during reaction, the spherical gas bubbles had a diameter of less than 10 nm. It can be assumed, that the gases with density of 3–10 atoms/nm³ could be detected only

inside large bubbles, whereby relatively high Be transparency for electron beam is favorable for this study.

It was confirmed that after deuterium implantation of beryllium at room temperature tiny (~1 nm in diameter) D_2 filled bubbles were formed (Chernikov et al., 1996). As driving force for bubble growth is gas pressure, formation of D_2 molecules was suggested. Moreover, the residual gas analysis has shown release of D_2 molecules during surface spattering. As far as hydrogen cannot form a molecule inside beryllium matrix, empty space is therefore required. Such space is provided during bubble growth.

4.3. Formation of Be–H compound on inner walls

As the spatial intensity distribution of the He line (Fig. 6) indicates, the inert gas fills the entire available volume of the bubble without interacting with internal walls. In contrast, an increase in the 13 eV peak at the bubble surface was observed, which structure does not show any measured difference to the bubble volume. Moreover, the spatial distance of ~2.5 nm between them and He peak on the interface demonstrates, that the 13 eV peak definitely comes from the bulk side (Fig. 3b). The measured thickness of this layer is about 4–5 nm, but its actual thickness can be estimated at < 2 nm taking into account the beam widening effect and deviation in bubble orientation. The spot size of the incident beam was about 1 nm, whereas the scattering reduces the lateral resolution to 2.0–2.5 nm. In addition, we do not really know if the internal basal surfaces are flat on atomic level or if they have several atomic steps inside. The 13 eV signal may indicate the absorption of H directly on the walls or may originate from BeH_2 plasmon. Unfortunately, we can neither confirm nor exclude the presence of the BeH_2 layer since we did not find any EELS references for BeH_2 .

In chemical compounds such as hydrides or hydroxides, H atoms do not behave as other elements. H atoms transfer single electrons into valence bands destroying typical H (or H_2) energy levels. For this reason, its direct detection inside solid states using EELS should be not possible. The indirect way used in the past is the detection of low loss spectra and the observation of changes of the plasmon position or core fine structures. For example, in (Paik et al., 2010), the in situ $ZrH_2 \rightarrow Zr$ phase transformation under electron beam was shown in TEM. The plasmon of the ZrH_2 phase at 14.6 eV becomes weaker, whereas the intensity of the plasmon located at 10.6 eV increased, which corresponds to metallic Zr. Similar behavior was also described for MgH_2 in (Surrey et al., 2016). In several publications, it was reported that extremely beam sensitive O–H bonding inside materials can be detected based on the pre peak at 532 eV in the O–K spectrum, which demonstrates the presence of gaseous O_2 (Klimenkov et al., 2008).

In (Blackmur et al., 2018) TEM observation of H trapping inside bubbles formed in ion irradiated zirconium was reported. Both, the presence of H inside bubbles and its absorption on the internal walls, were shown by spatially resolved EELS in nearly spherical faceted bubbles of the 7–10 nm size. The intensity of the H line is there remarkably smaller than in our case. The authors suggest that Zr–H bonds are of covalent nature so that H atoms could possess the required electrons to manifest the K edge, which is than visible in the EELS spectra. Nevertheless, the authors were not certain about the origin of the observed 13 eV peak and have also considered the surface plasmon as a possible explanation.

As shown in (Rocca, 1995) the energy of the surface plasmon ω_s can

Table 1
Data of quantitative calculations of He and H_2 gas inside bubbles of different size.

Bubble dimensions diameter/height (nm)	Cross-section He m ²	Cross-section H(atom) m ²	n_{He} atom*nm ³	n_{H_2} molecules*nm ³	pressure bar
75/32	(6,7 ± 1.0)*10 ⁻²⁴	(5,8 ± 0.9)*10 ⁻²⁴	11.9 ± 3.0	7.3 ± 2.2	720 ± 230
120/28	(6,7 ± 1.0)*10 ⁻²⁴	(5,8 ± 0.9)*10 ⁻²⁴	4.5 ± 1.2	6.4 ± 2.0	410 ± 120
160/19	(6,7 ± 1.0)*10 ⁻²⁴	(5,8 ± 0.9)*10 ⁻²⁴	4.2 ± 1.0	3.5 ± 1.1	290 ± 75

be calculated from the energy of the bulk plasmon ω_p by a simple equation:

$$\omega_s = \omega_p/\sqrt{2} \quad (3)$$

The measured bulk plasmon of $\omega_{p, Be} = 18.7$ eV 19.2 eV for Be corresponds to the values given in the previous publications (Diekmann et al., 1986; Soto et al., 2002). The surface plasmon in Be should then appear at $\omega_{s, Be} = 13.2$ eV nearly at the same energy as the H₂ line. The EELS investigations performed on the polycrystalline Be film reports the presence of surface plasmon peak at 12 eV 14 eV in beryllium layer (Soto et al., 2002). These results were also confirmed by (Sashin et al., 2001) where a surface plasmon at 13.2 eV was observed in 3 nm thick Be film. The similar energy and line shape of the H₂ line and surface plasmon in Be makes it harder to differentiate between them. It should also be not excluded, that both effects together contribute to an intensity increase on the basal planes. The surface plasmon at 13 14 eV was observed in cavities formed in materials even if H is not present. The round halo in He filled cavities was for example observed in implanted germanium (David et al., 2014).

However, the surface plasmon at 13 eV cannot explain both the surface effect and the presence of 13 eV peak in bubbles. The wide range delocalization of surface plasmon was reported only for the energies lower than 3 eV (Colliex et al., 2016). The delocalization of surface plasmon with energies higher than 10 eV comprises only a few nanometers. Its intensity drops to zero inside 10 nm tellurium nano road. In the present work the peak at 13 eV with intensity proportional to the volume seen by e beam was observed in many different gas filled bubbles with a thickness up to ~40 nm and diameter up to ~80 nm. For the second, no signal at 13 eV is present on the surface of bubbles opened during FIB preparation of lamellae. This measured absence of 13 eV in the open bubbles shows that the formation of the BeH₂ layer or H absorption is rather a convenient explanation for the origin of the 13 eV peak. Consequently, the increase in signal intensity of 13 eV on the walls of the bladder can tentatively be explained by the formation of Be–H bonds and not by a surface plasma. A conclusive differentiation between hydrogen adsorption at the surface or formation of BeH₂ cannot yet be made from the experiments. For these purposes, high resolution EELS (HR EELS) measurements are envisaged.

Finally, it is interesting to note that a recent multiscale modelling approach came to the conclusion that with increasing hydrogen coverage a substantial surface reconstruction occurs with a pronounced formation of Be H₂ Be H₂ unordered chains as first “surface layer” (Stihl and Vladimirov, 2016). Therefore, these modelling results suggest that the increase of the peak at 13 eV observed at the bubble walls comes from a BeH type bonding, while the signal from the bubble originates from molecular hydrogen.

5. Conclusions

EELS spectroscopy was used for detection and analysis of He and H₂ gases trapped inside flat hexagonal bubbles formed on the basal planes of beryllium under neutron irradiation. The peaks at 13.0 eV and 22.4 eV detected in the low loss EELS spectra suggest the presence of H₂ molecules and He atoms inside bubbles. The intensity increase of H line on the basal internal walls indicates strongly interaction of hydrogen with beryllium. However, the excitation of surface plasmons on the basal surfaces could also be the reason for 13 eV peak. Additional studies are required to clarify the nature of this surface effect. The number densities of both gases inside the bubbles were calculated using atomic scattering cross section and the intensity of the zero loss peak. The values He = (4.2 ± 1) at/nm³ and n_{H2} = (3.5 ± 1.2) molecules/nm³ were determined for a bubble with a diameter of 160 nm. The number densities of both gases increase with decreasing the bubble diameter.

Acknowledgments

This work has been carried out within the framework of the EUROfusion Consortium and has received funding from the Euratom research and training programme 2014 2018 and 2019 2020 under grant agreement No 633053. The views and opinions expressed herein do not necessarily reflect those of the European Commission.

References

- Ahn, C.C., Krivanek, O.L., Burgner, R.P., 1983. EELS Atlas: A Reference Guide of Electron Energy Loss Spectra Covering All Stable Elements. Center for Solid State Science Arizona State Univ., Tempe, Ariz 69 pp.
- Barabash, V., Eaton, R., Hirai, T., Kupriyanov, I., Nikolaev, G., Wang, Z., Liu, X., Roedig, M., Linke, J., 2011. Summary of beryllium qualification activity for ITER first-wall applications. Phys. Scr. Trans. 145, 14007.
- Blackmur, M.S., Dumbill, S., MacLaren, I., Hernandez-Maldonado, D., Styman, P.D., Gass, M., Nicholls, R.J., Hyde, J.M., Ramasse, Q.M., Annand, K.J., Smith, J.S., Gotham, N., 2018. The association of hydrogen with nanometre bubbles of helium implanted into zirconium. Scr. Mater. 152, 102–106.
- Chakin, V.P., Ye Ostrovsky, Z., 2002. Evolution of beryllium microstructure under high-dose neutron irradiation. J. Nucl. Mater. 307–311, 657–663.
- Chakin, V., Rolli, R., Moeslang, A., Klimenkov, M., Kolb, M., Vladimirov, P., Kurinskiy, P., Schneider, H.-C., van Til, S., Magielsen, A.J., Zmitko, M., 2013. Tritium release and retention properties of highly neutron-irradiated beryllium pebbles from HIDOB-01 experiment. J. Nucl. Mater. 442 (1–3), S483–S489.
- Chernikov, V.N., Alimov, V.K., Markin, A.V., Gorodetsky, A.E., Kanashenko, S.L., Zakharov, A.P., Kupriyanov, I.B., 1996. Gas-induced swelling of beryllium implanted with deuterium ions. J. Nucl. Mater. 233–237, 860–864.
- Cohen, H., Rez, P., Aoki, T., Crozier, P.A., Dellby, N., Dellby, Z., Gur, D., Lovejoy, T.C., March, K., Sarahan, M.C., Wolf, S.G., Krivanek, O.L., 2015. Hydrogen analysis by ultra-high energy resolution EELS. Microsc. Microanal. 21 (S3), 661–662.
- Colliex, C., Kociak, M., Stéphan, O., 2016. Electron energy loss spectroscopy imaging of surface plasmons at the nanometer scale. Ultramicroscopy 162, A1–A24.
- Condon, J.B., Schober, T., 1993. Hydrogen bubbles in metals. J. Nucl. Mater. 207, 1–24.
- Crozier, P.A., Chenna, S., 2011. In situ analysis of gas composition by electron energy-loss spectroscopy for environmental transmission electron microscopy. Ultramicroscopy 111 (3), 177–185.
- David, M.-L., Alix, K., Pailloux, F., Mauchamp, V., Couillard, M., Botton, G.A., Pizzagalli, L., 2014. In situ controlled modification of the helium density in single helium-filled nanobubbles. J. Appl. Phys. 115 (12), 123508.
- Diekmann, W., Eickmans, J., Otto, A., 1986. Plasmon dispersion in beryllium. Z. Phys. B: Condens. Matter 65 (1), 39–41.
- Egerton, R.F., 2011. Electron Energy-Loss Spectroscopy in the Electron Microscope, 3rd ed. Springer Science + Business Media LLC, Boston, MA.
- Fréchal, S., Walls, M., Kociak, M., Chevalier, J.P., Henry, J., Gorse, D., 2009. Study by EELS of helium bubbles in a martensitic steel. J. Nucl. Mater. 393 (1), 102–107.
- Hojou, K., Furuno, S., Kushita, K.N., Sasajima, N., Izui, K., 1998. EELS analysis of SiC crystals under hydrogen and helium dual-ion beam irradiation. Nucl. Instrum. Methods Phys. Res. B 141 (1–4), 148–153.
- Iakoubovskii, K., Mitsuishi, K., Nakayama, Y., Furuya, K., 2008. Mean free path of inelastic electron scattering in elemental solids and oxides using transmission electron microscopy: atomic number dependent oscillatory behavior. Phys. Rev. B 77 (10), 325.
- Jäger, W., Manzke, R., Trinkaus, H., Crecelius, G., Zeller, R., Fink, J., Bay, H.L., 1982. Density and pressure of helium in small bubbles in metals. J. Nucl. Mater. 111–112, 674–680.
- Jiang, W., Spurgeon, S.R., Zhu, Z., Yu, X., Kruska, K., Wang, T., Gigax, J., Shao, L., Senior, D.J., 2018. Chemical imaging and diffusion of hydrogen and lithium in lithium aluminate. J. Nucl. Mater. 511, 1–10.
- Klimenkov, M., Möslang, A., Lindau, R., 2008. EELS analysis of complex precipitates in PM 2000 steel. Eur. Phys. J. Appl. Phys. 42 (3), 293–303.
- Klimenkov, M., Chakin, V., Moeslang, A., Rolli, R., 2013a. TEM study of beryllium pebbles after neutron irradiation up to 3000appm helium production. J. Nucl. Mater. 443 (1–3), 409–416.
- Klimenkov, M., Möslang, A., Materna-Morris, E., 2013b. New method for detection of Li inside He bubbles formed in B10-alloyed steel after neutron irradiation. Micron (Oxford, England: 1993) 46, 51–56.
- Klimenkov, M., Chakin, V., Moeslang, A., Rolli, R., 2014. TEM study of impurity segregations in beryllium pebbles. J. Nucl. Mater. 455 (1–3), 660–664.
- Leapman, R.D., Sun, S., 1995. Cryo-electron energy loss spectroscopy: observations on vitrified hydrated specimens and radiation damage. Ultramicroscopy 59 (1–4), 71–79.
- Lu, Y., Yin, W.-J., Peng, K.-L., Wang, K., Hu, Q., Selloni, A., Chen, F.-R., Liu, L.-M., Sui, M.-L., 2018. Self-hydrogenated shell promoting photocatalytic H₂ evolution on anatase TiO₂. Nat. Commun. 9 (1), 2752.
- Manzke, R., Jäger, W., Trinkaus, H., Crecelius, G., Zeller, R., Fink, J., 1982. Quantitative determination of the pressure of He in bubbles in Al and Ni. Solid State Commun. 44 (4), 481–484.
- Möslang, A., Wiss, T., 2006. Materials for energy: from fission towards fusion. Nat. Mater. 5 (9), 679–680.
- Paik, B., Jones, I.P., Walton, A., Mann, V., Book, D., Harris, I.R., 2010. MgH₂ → Mg phase transformation driven by a high-energy electron beam: an in situ transmission

- electron microscopy study. *Philos. Mag. Lett.* 90 (1), 1–7.
- Pajuste, E., Vitins, A., Kizane, G., Zubkovs, V., Birjukovs, P., 2011. Tritium distribution and chemical forms in the irradiated beryllium pebbles before and after thermo-annealing. *Fusion Eng. Des.* 86 (9–11), 2125–2128.
- Rabaglino, E., Ronchi, C., Cardella, A., 2003. Recent progress in the modelling of helium and tritium behaviour in irradiated beryllium pebbles. *Fusion Eng. Des.* 69 (1–4), 455–461.
- Rocca, M., 1995. Low-energy EELS investigation of surface electronic excitations on metals. *Surf. Sci. Rep.* 22 (1–2), 1–71.
- Sashin, V.A., Bolorizadeh, M.A., Kheifets, A.S., Ford, M.J., 2001. Conduction band electronic structure of metallic beryllium. *J. Phys.: Condens. Matter* 13 (19), 4203–4219.
- Sernyaev, G.A., 2001. Radiation Damage Ability of Beryllium. Ekaterinburg Publishers.
- Soto, G., Díaz, J.A., Machorro, R., Reyes-Serrato, A., de La Cruz, W., 2002. Beryllium nitride thin film grown by reactive laser ablation. *Mater. Lett.* 52 (1–2), 29–33.
- Stihl, C., Vladimirov, P.V., 2016. Multiscale modelling of hydrogen behaviour on beryllium (0001) surface. *Nucl. Mater. Energy* 9, 547–553.
- Surrey, A., Schultz, L., Rellinghaus, B., 2016. Electron beam induced dehydrogenation of MgH₂ studied by VEELS. *Adv. Struct. Chem. Imaging* 2 (1), 526.
- Tao, R., Romanenko, A., Cooley, L.D., Klie, R.F., 2013. Low temperature study of structural phase transitions in niobium hydrides. *J. Appl. Phys.* 114 (4), 44306.
- Vladimirov, P., Bachurin, D., Borodin, V., Chakin, V., Ganchenkova, M., Fedorov, A., Klimenkov, M., Kupriyanov, I., Moeslang, A., Nakamichi, M., Shibayama, T., van Til, S., Zmitko, M., 2014. Current status of beryllium materials for fusion blanket applications. *Fusion Sci. Technol.* 66 (1), 28–37.
- Vladimirov, P., Ferrero, C., Chakin, V., Kurinskiy, P., Moeslang, A., Pieritz, R., Weitkamp, T., Brun, E., 2015. Microstructure of out-of-pile annealed neutron irradiated beryllium studied by X-ray tomography. *Acta Mater.* 88, 293–301.
- Walsh, C.A., Yuan, J., Brown, L.M., 2000. A procedure for measuring the helium density and pressure in nanometre-sized bubbles in irradiated materials using electron-energy-loss spectroscopy. *Philos. Mag. A* 80 (7), 1507–1543.
- Yakovlev, S., Misra, M., Shi, S., Libera, M., 2009. Specimen thickness dependence of hydrogen evolution during cryo-transmission electron microscopy of hydrated soft materials. *J. Microsc.* 236 (3), 174–179.